ChemComm

Phenylene as an Efficient Mediator for Intermetallic Electronic Coupling

SCHOLARONE™
Manuscripts

COMMUNICATION

Phenylene as an Efficient Mediator for Intermetallic Electronic Coupling

Lyndsy A. Miller-Clark, Adharsh Raghavan, Reese A. Clendening and Tong Ren*

The new compound $[(NC)Ru_2(ap)_4]_2(\mu\text{-}1,4\text{-}C_6H_4)$ (ap = 2-anilinopyridinate) was prepared to address the open question of whether a 1,4-phenylene bridge can mediate intermetallic electronic coupling. As a manifestation of strong coupling, hole delocalization between the Ru_2 centers on the IR time scale (10^{-14} s) was established using spectroelectrochemistry. An orbital mechanism for coupling was elaborated with DFT analysis.

Conjugated organometallic compounds are promising building blocks for soft functional materials,[1-3] where the extensive $d\pi$-π interactions render rich redox and optical properties unattainable in pure organic systems. Polymers based on metal-alkynyl units, polymetallaynes (**I** in Chart 1), are particularly attractive as electronic materials due to their structural rigidity, reduced band gaps and excellent charge mobility.[3-5] Correspondingly, the charge transfer processes across metal-acetylide backbones in mono- and bimetallic compounds have been extensively probed based on mixed-valency therein, and the structure-property relationships derived provide useful insight for material design.[6-8] Metal-acetylide motifs with proven proficiency in mediating charge transfer have been incorporated into nano-junctions with substantial conductance,[9,10] and have been shown to function as switches[11] and flash-like memory devices.[12] While the scope of metal-aryl chemistry is immense due to its relevance to cross coupling reactions,[13] polymetallaarylenes (**II** in Chart 1) have yet to be used for material applications. Furthermore, intermetallic coupling across a simple metal-(μ-1,4-phenylene)-metal backbone has never been experimentally demonstrated.

Diruthenium paddlewheel type compounds are well known for their robust redox responses.[14,15] Facile charge delocalization
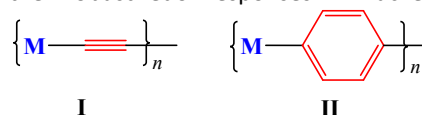
Chart 1 Polymetallaynes (**I**) and polymetallaarylene (**II**) structural motifs.

across the bridging oligoyn-diyl (C_{2n}) has been demonstrated in $[Ru_2(ap)_4]_2(\mu\text{-}C_{2n})$ type compounds (ap = 2-anilinopyridinate) through Vis-NIR spectroelectrochemical (SEC) experiments in bulk solutions.[16,17] The rich redox characteristics of Ru_2 compounds further enable a broad range of applications as wires in nano-junctions,[18,19] spin-chains,[20] and catalytic activation of small molecules.[21-23] More recently, $Ru_2(ap)_4(Ar)$ type compounds (Ar = aryl) were prepared,[24] and their capacity in binding small linear ligands such as CO, CN^- and C_2H^- at the axial site *trans*- to Ar was demonstrated.[25] Interested in expanding this chemistry to investigate bridging arylenes, we report herein the formation and characterization of $[Ru_2(ap)_4]_2(\mu\text{-}1,4\text{-}C_6H_4)$ (**1**, Scheme 1) and its derivative $[(NC)Ru_2(ap)_4]_2(\mu\text{-}1,4\text{-}C_6H_4)$ (**2**, Scheme 1), the unambiguous evidence of strong intermetallic coupling across the phenylene bridge through the SEC study of $[\mathbf{2}]^+$, and companion DFT and TD-DFT analyses.
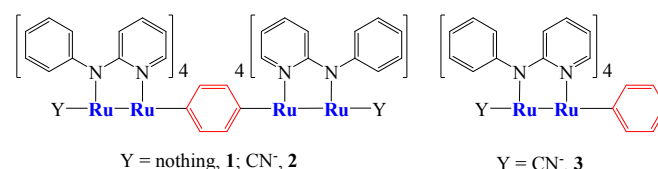
Scheme 1 Compounds discussed in this work.

As detailed in the ESI, the reaction of $Ru_2(ap)_4Cl$ with a slight excess of 1,4-dilithiobenzene yielded the phenylene bridged

Department of Chemistry, Purdue University, West Lafayette, Indiana 47907
Email: tren@purdue.edu

compound **1** (62%), and its 'dimeric' nature was verified by the isotopic distribution of Ru in the ESI-MS of **1** (Fig. S1, ESI). Efforts to probe **1** spectroscopically were thwarted by its high sensitivity to air / moisture and low solubility in organic solvents. Seeking a more stable form of the dimer, **1** was treated with [Bu$_4$N][CN] under N$_2$, which was followed by exposure to O$_2$ to yield **2** (59%). Compound **2**, a dimer of Ru$_2$(III,III) units, is air-stable and significantly more soluble than **1**. In order to benchmark electronic properties of **2**, the corresponding 'monomer' (NC)Ru$_2$(ap)$_4$(C$_6$H$_5$) (**3**) was prepared from Ru$_2$(ap)$_4$(C$_6$H$_5$)[24] using the same procedure as for **2**.

Both the dimeric nature of **2** and the phenylene bridging are unambiguously established with the single crystal X-ray structure of **2** shown in Fig. 1, with key metric parameters also provided. The Ru$_2$ units in **2** display significant distortions from an idealized uniaxial paddlewheel structure as exemplified by the large deviation of Ru–Ru–C$_{ph}$ from linearity, which is likely caused by a second order Jahn-Teller effect.[25] Both the Ru–Ru (*ca.* 2.49 Å) and Ru–C$_{aryl}$ (*ca.* 2.05 Å) bond lengths closely match those found for the monomer **3** (Ru–Ru, 2.50 Å; Ru–C$_{aryl}$, 2.05 Å; Fig. S4 and Tables S1–S2, ESI), indicating similar electronic structures around the Ru$_2$ core between **2** and **3**.
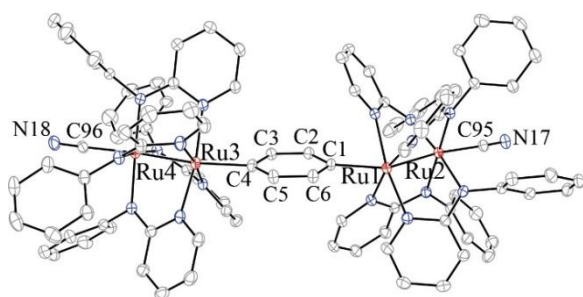
Fig. 1 ORTEP plot of **2** at 30% probability level. Selected bond lengths (Å) and angles (deg): Ru2–Ru1, 2.4892(3); Ru4–Ru3, 2.4829(3); Ru1–C1, 2.052(3); Ru3–C4 2.051(3); Ru2–C95, 2.019(3); Ru4–C96, 2.013(3); Ru2–Ru1–C1, 152.21(9); Ru4–Ru3–C4, 147.14(9); Ru1---Ru3, 6.95(4).

Electronic coupling mediated by phenylene in **2** was first probed with voltammetric analysis. As shown in Fig. 2, compound **3** exhibits two reversible 1e$^-$ Ru$_2$-based couples: an oxidation **A** at 0.21 V (*versus* Fc$^{+/0}$) and a reduction **B** at -0.92 V, which is a characteristic common to Ru$_2$(III,III) species supported by the ap scaffold.[25,26] Compound **2** exhibits two 1e$^-$ oxidations at potentials close to that of **A** in **3**: 0.29 (**A2**) and 0.01 V (**A1**), and two 1e$^-$ reductions at potentials close to that of **B** in **3**: -0.91 (**B1**) and -1.09 V (**B2**). A reduction event (**C**) beyond **B2** is attributed to a species derived from degradation of [**2**]$^{2-}$. The stepwise appearance for the redox couples in **2** is a hallmark of significant intermetallic coupling through the bridging ligand.[27] Furthermore, the $\Delta E_{1/2}$(+1) (calculated as: $E_{1/2}$(**A2**) - $E_{1/2}$(**A1**)) of **2**, 291 mV, is slightly higher than that reported for [Ru$_2$(ap)$_4$]$_2$(μ-C$_2$) (280 mV),[16] suggesting that the coupling in [**2**]$^+$ may be substantial. On the other hand, the $\Delta E_{1/2}$(-1) ($E_{1/2}$(**B1**) - $E_{1/2}$(**B2**); 174 mV) of **2** is much smaller than

that of [Ru$_2$(ap)$_4$]$_2$(μ-C$_2$) (660 mV) (further comparisons in Table S6, ESI), hinting that the phenylene is less efficient in mediating coupling in [**2**]$^-$. It is worth mentioning that voltammograms of compound **1** (Fig. S5, ESI), though less-than-ideal due to low solubility, also display the pattern of pairwise oxidations and reductions similar to that of **2**.
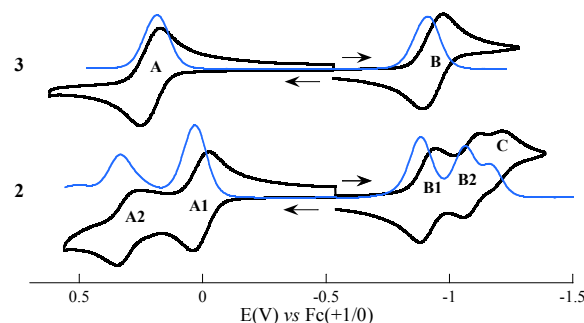

Fig. 2 Cyclic (black) and differential pulse (blue) voltammograms of compounds **2** and **3** (1.0 mM) recorded in 0.1 M Bu$_4$NPF$_6$ in THF at a scan rate of 0.100 V/s.

To quantify the degree of electronic coupling in **2**, mixed valency in both [**2**]$^+$ and [**2**]$^-$ were probed with Vis-NIR and IR SEC experiments and compared with that of the monomer molecule, **3**. As shown in Fig. 3, both compounds **2** and **3** display an intense peak around 550 nm (18,350 cm^{-1}, band I), which is assigned to π(Ru$_2$) → π*(N)/δ*(Ru$_2$).[28] Compound **3** also absorbs strongly around 950 nm (10,500 cm^{-1}, band II), and the analogous peak in **2** is shifted to 1025 nm (9,900 cm^{-1}), which are likely the transitions between HOMO and LUMO (π*(Ru$_2$) → δ*(Ru$_2$), see the DFT discussion below).

Upon the first 1e$^-$ reduction of **2**, both bands I and II are blue shifted with reduced intensities (Fig. S7a, ESI). On the second 1e$^-$ reduction, both bands are further blue shifted with the former intensifying and the latter weakening (Fig. S7b, ESI). Significantly, there is no discernible peak emerging in the red-NIR region, hinting at the localized nature of [**2**]$^-$ despite a sizable $\Delta E_{1/2}$(-1). Furthermore, two distinctive ν(C≡N) (2092 and 2069 cm^{-1}) were located in the IR SEC of [**2**]$^-$ (Fig. S14, ESI), which clearly confirms localization of the added electron on the IR time scale.[27]

Upon the first 1e$^-$ oxidation of **2**, both bands I and II are red shifted with II intensified. Very intriguingly, an intense new band (III) grows in with an onset around 5,800 cm^{-1}. Because of the cutoff of the NIR spectrometer (2400 nm, 4167 cm^{-1}), only half of band III is recorded in the NIR SEC. Fortunately, much of the remaining half of band III is located in the IR SEC of [**2**]$^+$ (Fig. 3a and Fig. S12, ESI), from which a nearly complete peak is constructed for band III. On the second 1e$^-$ oxidation, band III is completely bleached (Fig. 3b), while bands I and II further intensified. As a baseline study, the SEC of the first 1e$^-$ oxidation of **3** was recorded (Fig. 3c), where both bands I and II are red shifted with the latter slightly intensified, similar to those of [**2**]$^+$. Nonetheless, there is no new significant peak

emerging for [**3**]$^+$ in the NIR-IR region. Hence, the absence of band III in both [**2**]$^{+2}$ and [**3**]$^+$ establishes it as an intervalence charge-transfer transition (IVCT).[6,27,29]
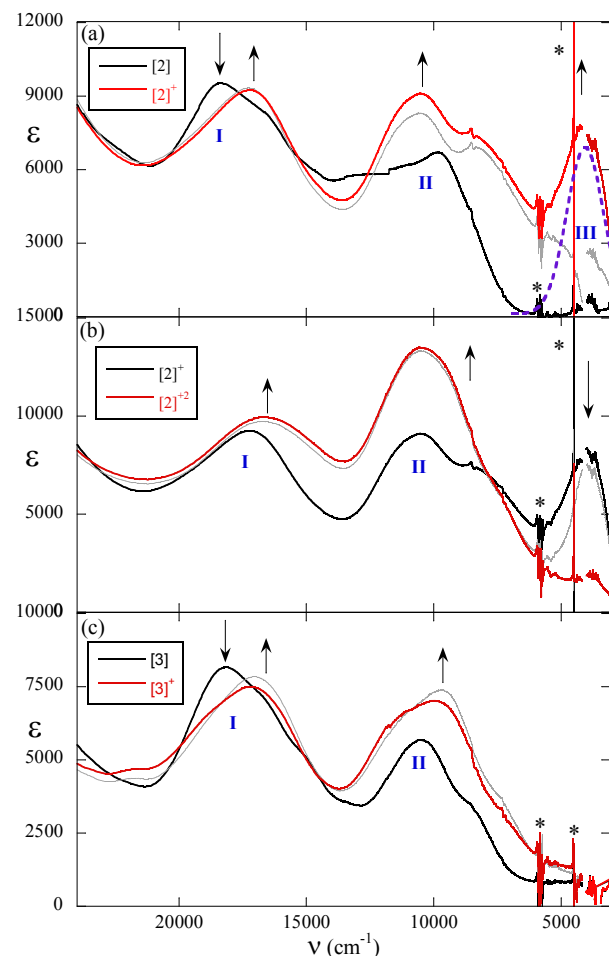

Fig. 3 Vis-NIR and IR spectroelectrochemistry of **2** with Gaussian fit of the IVCT band (purple dash) at 0.4 V (a), 0.65 V (b) and of **3** at 0.3 V (c) vs Ag wire, 2 mM analyte with 0.1 M Bu$_4$NPF$_6$ in THF in all cases. Instrument artifacts / solvent overtones noted as * and grey lines used to denote intermediate scans for each SEC experiment.

Further analysis of the IVCT band is enabled with Gaussian deconvolution of the Vis-NIR and IR SEC of [**2**]$^+$, which yields the following parameters for the fit (purple dash in Fig. 3a): ν_{IVCT} = 4,050 cm^{-1}, ε = 6,860 M^{-1} cm^{-1}, $\Delta\overline{\nu}_{1/2}$ = 1,716 cm^{-1} (Figs. S8–S11, ESI). Importantly, the $\Delta\overline{\nu}_{1/2}$ is significantly smaller than the predicted value by the Hush model ($\Delta\overline{\nu}_{1/2}$(Hush) = (2310 ν_{IVCT})$^{1/2}$ = 3,060 cm^{-1}),[29] which, along with the large ε, suggests that [**2**]$^+$ is a highly delocalized (Robin-Day class III) mixed valence species. Further evidence cementing this assessment is the IR SEC of [**2**]$^+$ (Fig. S13, ESI) that consists of a single and narrow C≡N stretch peak ($\Delta\overline{\nu}_{1/2} \sim$ 8 cm^{-1}; in comparison, $\Delta\overline{\nu}_{1/2}$(C≡N) in [**3**]$^+$ ~ 15 cm^{-1} (Fig. S16, ESI)), indicating that two Ru$_2$ cores are equivalent on the IR time scale (10^{-14} s).[27] The lower threshold of the electronic coupling element H_{AB} can be calculated based on the above mentioned IVCT band

parameters and a Ru3---Ru1 distance (r) of 6.95 Å with the Mulliken-Hush equation:[6,29]

$$H_{AB} = (0.0206/r)(\nu_{IVCT}\,\Delta\overline{\nu}_{1/2}\varepsilon)^{1/2} = 647\ cm^{-1}$$

To understand the underlying orbital mechanism for the observed Ru$_2$—Ru$_2$ coupling in [**2**]$^+$, DFT calculations were performed for **2**, [**2**]$^+$ and **3**. Our previous work[25] with (Y)Ru$_2$(ap)$_4$(C$_6$H$_4$-4-NMe$_2$) indicated that the addition of axial ligands alters the ground state electron configuration (see note in ESI, Fig S20) from $\sigma^2\pi^4\delta^2(\pi^*\delta^*)^3$ in Ru$_2$(ap)$_4$(Ar) to either "$\pi^4\delta^2(\pi^*)^4$" (Y = CN) or "$\pi^4\delta^2(\pi^*)^4\delta^*$" (Y = CO). Magnetic susceptibility measurements using the Evans method[30] yielded effective magnetic moments at 293 K of 2.18 and 2.26 μ_B for **2** and **3**, respectively (Table S8, ESI). Both compounds contain [Ru$_2$(ap)$_4$]$^{2+}$ cores in the Ru$_2$(III,III) oxidation state, which is expected to be diamagnetic (S = 0 ground state). Population of a higher spin state (S = 1) is unusual for this class of compounds, but not unprecedented.[25,31] A possible explanation for this is an extensive mixing between a [$\pi_{xz}^2\pi_{yz}^2\delta^2(\pi_{xz}^*)^2(\pi_{yz}^*)^2$]$_2$ singlet and a [$\pi_{xz}^2\pi_{yz}^2\delta^2(\pi_{xz}^*)^2$]$_2(\pi_{yz,1}^*)^2\pi_{yz,2}^*\delta^*$ triplet (phenylene moiety is parallel to the xz plane). DFT calculations on **2** and **3** predicted a singlet-triplet energy gap of 0.87 kcal/mol and 2.0 kcal/mol, respectively. Such small barriers indicate that a large population of the triplet state may be feasible, or that the ground state has some multireference character.
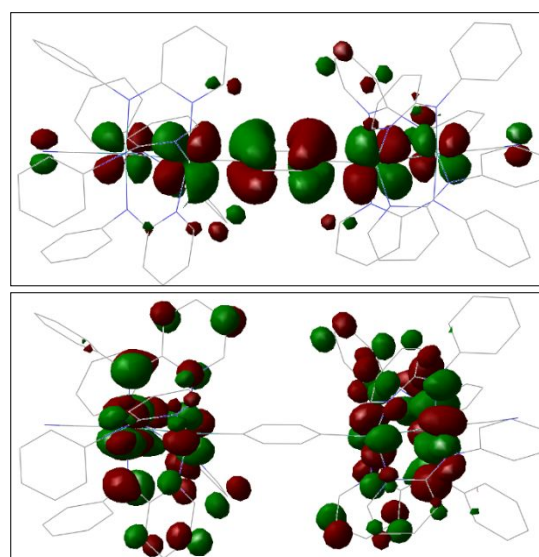
Fig. 4 HOMO (top) and LUMO (bottom) of the DFT-optimized structure of **2**. |Isovalue| = 0.020.

Mulliken orbital composition analysis of the frontier orbitals of **2** (Fig. 4) reveals that its HOMO is primarily composed of the antibonding combination of π^*(Ru-Ru) (62%) and π(Ph) orbitals (25%). On the other hand, the LUMO mainly consists of the δ^*(Ru-Ru) on the Ru$_2$ cores (49% Ru contribution), with < 0.5% contribution from the bridging phenylene unit (Table S13, ESI). DFT calculations on the 1e$^-$ oxidized [**2**]$^+$ predict an

electronic configuration of "$[\pi_{xz}^2\pi_{yz}^2\delta^2(\pi_{xz}^*)^2]_2(\pi_{yz}^*)^3$" with the HOMO in **2** becoming the SOMO (singly occupied molecular orbital). The electronic configuration of [**2**]$^-$ is computed as $[\pi_{xz}^4\pi_{yz}^2\delta^2(\pi_{xz}^*)^2(\pi_{yz}^*)^2]_2\delta^*$ with the LUMO in **2** becoming the SOMO; the absence of phenylene contribution explains the lack of coupling in [**2**]$^-$. This accounts for the SEC observations: i.e., [**2**]$^+$ exhibits an IVCT band in the NIR region, whereas [**2**]$^-$ does not.

Time-dependent DFT calculations (TD-DFT) on [**2**]$^+$ indicate that the observed IVCT band corresponds to a transition (calculated at 4,647 cm^{-1}) from an orbital that is primarily a *bonding* combination of π^*(Ru-Ru) (43.2% Ru *d*) and π(Ph) (7.2% C p_y) to the above-mentioned SOMO of [**2**]$^+$ (Figs. S21–S22, ESI). In comparison, the previously studied [Ru$_2$(ap)$_4$]$_2$(μ-C$_{2n}$) series ([Ru$_2$(II,III)]$_2$) have the localized δ^* orbitals as SOMO/SOMO-1, while the antibonding combination of π^*(Ru-Ru) and π(C≡C) are of lower energies.[16,17] Clearly, the phenylene (C$_6$H$_4$$^{2-}$) is a much stronger *π-base* ligand than oligoyn-diyl (C$_{2n}$$^{2-}$), and pushes π^*(Ru-Ru) up to HOMO / SOMO, enabling intermetallic coupling by a mechanism different from those of M-C$_{2n}$-M.

In conclusion, two new phenylene-bridged compounds, [(Y)Ru$_2$(ap)$_4$]$_2$(μ-1,4-C$_6$H$_4$) (Y = nothing or CN$^-$), were prepared and characterized. Both Vis-NIR and IR SEC studies of [**2**]$^+$ reveal its nature as a class III Robin-Day mixed valent ion with the hole being delocalized on the IR time scale (10^{-14} s). DFT analysis provides a rationale for the efficacy of the phenylene bridge in mediating hole transfer over electron transfer, while TD-DFT calculations reveal the origin of the IVCT band. While the intermetallic coupling mediated by arylene in a cyclo-metallated *N,C,N*-tridentate ligand was demonstrated in the pioneering studies of Sauvage and Launay,[32,33] this study provides the first unambiguous demonstration of strong coupling between metal units via plain phenylene bridge. In-depth understanding of magnetism, distance dependence, variation of ap backbone, and further DFT analysis are in the scope of future work.

Notes and references

1   G. R. Whittell, M. D. Hager, U. S. Schubert and I. Manners, *Nature Mater.*, 2011, **10**, 176-188.
2   A. Winter and U. S. Schubert, *Chem. Soc. Rev.*, 2016, **45**, 5311-5357.
3   V. W.-W. Yam, A. K.-W. Chan and E. Y.-H. Hong, *Nature Rev. Chem.*, 2020, **4**, 528-541.
4   W.-Y. Wong and C.-L. Ho, *Acc. Chem. Res.*, 2010, **43**, 1246-1256.
5   C.-L. Ho, Z.-Q. Yu and W.-Y. Wong, *Chem. Soc. Rev.*, 2016, **45**, 5264-5295.
6   J.-P. Launay, *Chem. Soc. Rev.*, 2001, **30**, 386-397.
7   A. Haque, R. A. Al-Balushi, I. J. Al-Busaidi, Muhammad S. Khan and P. R. Raithby, *Chem. Rev.*, 2018, **118**, 8474-8597.
8   M. R. Bryce, *J. Mater. Chem. C*, 2021, **9**, 10524-10546.
9   T. L. Schull, J. G. Kushmerick, C. H. Patterson, C. George, M. H. Moore, S. K. Pollack and R. Shashidhar, *J. Am. Chem. Soc.*, 2003, **125**, 3202-3203.
10   Y. Tanaka, Y. Kato, T. Tada, S. Fujii, M. Kiguchi and M. Akita, *J. Am. Chem. Soc.*, 2018, **140**, 10080-10084.
11   F. B. Meng, Y. M. Hervault, Q. Shao, B. H. Hu, L. Norel, S. Rigaut and X. D. Chen, *Nature Commun.*, 2014, **5**, Art. Number 3023.
12   H. Zhu, S. J. Pookpanratana, J. E. Bonevich, S. N. Natoli, C. A. Hacker, T. Ren, J. S. Suehle, C. A. Richter and Q. Li, *ACS Appl. Mater. Interfaces*, 2015, **7**, 27306-27313.
13   D. Alberico, M. E. Scott and M. Lautens, *Chem. Rev.*, 2007, **107**, 174-238.
14   M. Cortijo, R. González-Prieto, S. Herrero, J. L. Priego and R. Jiménez-Aparicio, *Coord. Chem. Rev.*, 2019, **400**, Art. No. 213040.
15   E. Van Caemelbecke, T. Phan, W. R. Osterloh and K. M. Kadish, *Coord. Chem. Rev.*, 2021, **434**, Article 213706.
16   G. L. Xu, G. Zou, Y. H. Ni, M. C. DeRosa, R. J. Crutchley and T. Ren, *J. Am. Chem. Soc.*, 2003, **125**, 10057-10065.
17   Z. Cao, B. Xi, D. S. Jodoin, L. Zhang, S. P. Cummings, Y. Gao, S. F. Tyler, P. E. Fanwick, R. J. Crutchley and T. Ren, *J. Am. Chem. Soc.*, 2014, **136**, 12174-12183.
18   A. S. Blum, T. Ren, D. A. Parish, S. A. Trammell, M. H. Moore, J. G. Kushmerick, G.-L. Xu, J. R. Deschamps, S. K. Pollack and R. Shashidhar, *J. Am. Chem. Soc.*, 2005, **127**, 10010-10011.
19   S. Ogawa, S. Chattopadhyay, Y. Tanaka, T. Ohto, T. Tada, H. Tada, S. Fujii, T. Nishino and M. Akita, *Chem. Sci.*, 2021, **12**, 10871-10877.
20   S. D. Su, X. Q. Zhu, Y. H. Wen, L. T. Zhang, Y. Y. Yang, C. S. Lin, X. T. Wu and T. L. Sheng, *Angew. Chem. Int. Ed.*, 2019, **58**, 15344-15348.
21   T. Miyazawa, T. Suzuki, Y. Kumagai, K. Takizawa, T. Kikuchi, S. Kato, A. Onoda, T. Hayashi, Y. Kamei, F. Kamiyama, M. Anada, M. Kojima, T. Yoshino and S. Matsunaga, *Nature Cat.*, 2020, **3**, 851-858.
22   M. J. Trenerry, C. M. Wallen, T. R. Brown, S. V. Park and J. F. Berry, *Nature Chem.*, 2021, **13**, 1221-1227.
23   J. F. Berry and C. C. Lu, *Inorg. Chem.*, 2017, **56**, 7577-7581.
24   A. Raghavan, B. L. Mash and T. Ren, *Inorg. Chem.*, 2019, **58**, 2618-2626.
25   A. Raghavan, F. Yuan and T. Ren, *Inorg. Chem.*, 2020, **59**, 8663-8666.
26   T. Ren, *Organometallics*, 2005, **24**, 4854-4870.
27   K. D. Demadis, C. M. Hartshorn and T. J. Meyer, *Chem. Rev.*, 2001, **101**, 2655-2686.
28   A. R. Corcos, M. D. Roy, M. M. Killian, S. Dillon, T. C. Brunold and J. F. Berry, *Inorg. Chem.*, 2017, **56**, 14662-14670.
29   B. S. Brunschwig, C. Creutz and N. Sutin, *Chem. Soc. Rev.*, 2002, **31**, 168-184.
30   D. F. Evans, *J. Chem. Soc.*, 1959, 2003-2005.
31   G. M. Chiarella, F. A. Cotton, C. A. Murillo, K. Ventura, D. Villagran and X. Want, *J. Am. Chem. Soc.*, 2014, **136**, 9580-9589.
32   J.-P. Sutter, D. M. Grove, M. Beley, J.-P. Collin, N. Veldman, A. L. Spek, J.-P. Sauvage and G. van Koten, *Angew. Chem. Int. Ed.*, 1994, **33**, 1282-1285.
33   C. Patoux, J.-P. Launay, M. Beley, S. Chodorowski-Kimmes, J.-

ChemComm

P. Collin, S. James and J.-P. Sauvage, *J. Am. Chem. Soc.*, 1998, **120**, 3717-3725.